











## Highlights

### **A Paradigm Shift to Assembly-like Finite Element Model Updating**

Gabriele Dessena , Alessandro Pontillo , Dmitry I. Ignatyev , James F. Whidborne , Luca Zanotti Fragonara 

- Assembly-like finite element model updating is proposed and validated on a wing model;
- The correlation between the finite element model and the experimental results is improved by 20%;
- The proposed approach halves the computational cost and offers comparable precision to standard approaches.

# A Paradigm Shift to Assembly-like Finite Element Model Updating

Gabriele Dessena <sup>a,b</sup>, Alessandro Pontillo <sup>b</sup>, Dmitry I. Ignatyev <sup>a</sup>, James F. Whidborne <sup>a</sup>, Luca Zanotti Fragonara <sup>a</sup>

<sup>a</sup>*School of Aerospace, Transport and Manufacturing, Cranfield University, College Road, Cranfield, MK43 0AL, England, UK*

<sup>b</sup>*Department of Aerospace Engineering, Universidad Carlos III de Madrid, Av.da de la Universidad 30, 28911, Leganés, Madrid, Spain*

<sup>c</sup>*School of Engineering, UWE Bristol, Frenchay Campus, Coldharbour Lane, Bristol, BS16 1QY, England, UK*

---

## Abstract

In general, there is a mismatch between a finite element model of a structure and its real behaviour. In aeronautics, this mismatch must be small because finite element models are a fundamental part of the development of an aircraft and of increasing importance with the trend to more flexible wings in modern designs. Finite element model updating can be computationally expensive for complex structures and surrogate models can be employed to reduce the computational burden. A novel approach for finite element model updating, namely assembly-like, is proposed and validated using real experimental data. The assembly-like model updating framework implies that the model is updated as parts are assembled. Benchmarking against the classical global, or one-shot, approach demonstrates that the proposed method is more computationally efficient since it takes 20% fewer iterations to obtain convergence, also using fewer parameters for the model evaluations. Despite the increase in computational performance, the new approach retains the fidelity of the global approach.

*Keywords:* Finite element model updating, Flexible wings, High aspect ratio, Aeronautical structures, Optimisation, Kriging

---

## Nomenclature

### *Definitions, Acronyms and Abbreviations*

A: Area	L: Length
AR: Aspect Ratio	$M$ : Mass Matrix
BearDS: Beam Reduction Dynamic Scaling	MAC: Modal Assurance Criterion
E: Young Modulus	MTMAC: Modified Total Modal Assurance Criterion
EGO: Efficient Global Optimization	P: Static Load
$C$ : Damping Matrix	rEGO: refined Efficient Global Optimisation
$\bar{c}$ : Mean Aerodynamic Chord	RMS: Root Mean Square
EGO: Efficient Global Optimization	XB-2: eXperimental BearDS-2
EI: Expected Improvement	$x_n$ : Optimisation Variable
$EI$ : Bending Stiffness	$\alpha$ : Mass Proportional Rayleigh Damping Coefficient
EMA: Experimental Modal Analysis	$\beta$ : Stiffness Proportional Rayleigh Damping Coefficient
FEM: Finite Element Model	$\delta_{tip}$ : Tip Deflection
FEMU: Finite Element Model Updating	$\zeta_n$ : Damping Ratio
FEMU_1: FEM Updated via Bottom-up	$\lambda$ : Taper Ratio
FEMU_2: FEM Updated via Top-down	$\Lambda_{c/4}$ : Quarter-chord Sweep Angle
GA: Genetic Algorithm	$\Lambda_{LE}$ : Leading Edge Sweep Angle
GVT: Ground Vibration Testing	$\rho$ : Density
HAR: High Aspect Ratio	$\phi_n$ : Mode Shape
I: Moment of Inertia	$\omega_n$ : Natural Frequency
J: Torsion Constant	

## 1. Introduction

Over the last three decades, increasing computational power has allowed for the rapid development of finite element model updating (FEMU) methods [1]. This is because a general mismatch between the finite element models (FEMs) and the real systems they are meant to describe usually exists.

In [2], FEMU techniques are divided into two categories: direct and indirect methods. The former is not suitable for practical engineering applications as (i) they require very precise measurements of the structural vibration response, (ii) have a high sensitivity to noise, (iii) cannot be used with truncated data and (iv) are prone to lose symmetry in the FEM matrix. However, indirect, or iterative, methods accommodate these drawbacks. Moreover, iterative methods, driven by the minimisation of penalty functions, can require a heavy computational burden. This happens for evolutionary techniques, such as genetic algorithms (GAs) [3]. Hence, surrogate-based techniques can be employed for more efficient use of computational power. This is done in [4] for the FEMU of numerical and benchmark structures using the well-known efficient global optimization (EGO) on frequency domain data. In order to improve the local capabilities of a global algorithm like EGO, an enhanced version of EGO, the refined efficient global optimisation (rEGO) has been proposed in [5, 3]. rEGO was successfully applied to numerical and experimental systems for damage detection via FEMU. The reader interested in a more comprehensive review on FEMU can refer to [6] and [7], while for thorough reviews of indirect methods, the works of [8] and [2] are suggested.

The FEMU task is important across all fields of engineering, finding applications such as damage detection [9] and identification [10]. FEMU is also crucial in aeronautics, where having a reliable FEM is pivotal in meeting certification requirements [11]. Further challenges have recently arisen for FEMU in aeronautics, in particular for aircraft wings, because the design paradigm is shifting towards lightweight materials and slenderer wings, in order to improve their aerodynamic efficiency [12]. Hence, developing accurate models is not only necessary for analysing aeroelastic effects, but also for design and controls. In particular, [13] develop a FEM of a scaled aircraft model to be updated with ground vibration testing (GVT) data from different loaded scenarios to estimate flutter onset speed. In [14] a FEMU technique is implemented for positioning a wing box composite material layers for passive aeroelastic suppression, while in [15] model updating is used for enhancing the handling qualities of an aircraft with flexible wings. FEMU has also been implemented for other applications, such as reverse engineering of a fighter aircraft internal structure [16]. Nevertheless, FEMU, in aeronautics, is not only carried out on wings, but also on the full aircraft, e.g. [17], and components, e.g. [18].

Experimental data is required to update a FEM and in most cases, results from vibration data are used. The most prominent product of vibration data are modal parameters [19], which can be obtained by experiment, the so-called experimental modal analysis (EMA) [20], and during normal operation, known as operational modal analysis [21]. A particular type of EMA, used in aeronautics, is GVT and in this work, the two terms are used interchangeably as the work deals with aeronautical structures. In fact, modal parameters, in particular, natural frequencies ( $\omega_n$ ) and mode shapes ( $\phi_n$ ) are a common metric for FEMU [23]. Notably, [24] used  $\phi_n$ , via the modal assurance criterion (MAC) [25], from operational data for the FEMU of a wing section. Nevertheless, approaches based on the direct use of experimental data are still common, such as in [22] where a series of nonlinear case studies models has been updated using time domain responses.

Having an accurate structural model of an aircraft structure is not fundamental only for the structural assessment per se, but also for the general life-cycle assessment of the aircraft. Recent advances in the digital twin paradigm have shown that this is vital for building reliable models [26]. These challenges are more challenging nowadays as wings become more flexible. For example, [27, 28] proposes a method for the numerical extraction of modal data from deformed wings (vertical displacement of the wing); however, this was not further explored experimentally. In [29] a component-based FEMU strategy is applied to a composite wing aircraft. Instead of updating the complete structure, the updating is carried out for an individual component, before assembly into the whole system; however, no comparison is given to one-shot approaches, neither in terms of performance nor precision. The latter is addressed, on the same system, in [30], showing favourable results, computationally speaking, for the progressive approach. However, the implementation suggested by Zhao in the aforementioned works, in particular their intermediate steps, is more similar to a hybrid testing approach [31, 32], as usually defined within Civil Engineering, where only part of a structure, or system (e.g. the port wing), is known, rather than to an assembly-like procedure. In fact, EMA data is available only for the wing and for the full assembly, rather than for all the components. Notably, a similar application is carried out for the structural health monitoring of a suspended bridge model in [33]. Nevertheless, from these works

it became apparent that the possibility of carrying out assembly-like model assembly, or updating, is appealing as one can consider smaller, in terms of computational loads (e.g. nodes and elements), models, rather than larger and more complex ones. However, a more dedicated approach to the paradigm shift from one-shot and partial model approaches to progressive assembly-like approaches is needed, since these works have not addressed the stepwise characterisation of all subassemblies.

In order to establish the feasibility, goodness and efficiency of this method, a comparison between the proposed assembly-like and the traditional direct approaches is needed. This comparison should verify the performance, in terms of model improvement, and its efficiency, in terms of computational power used (so model complexity) and iterations needed for convergence.

Given the aforementioned motivation, the novelty of this work is to propose and assess a framework for the assembly-like FEMU against the classical direct approach to show its goodness and efficiency. The framework will be tested on a flexible wing model, of which thorough experimental data, involving the full wing and its parts and sub-assemblies, is available in [34, 35]. The hypothesis is that there could be an improvement in model accuracy and computational performance compared to traditional one-shot approaches. The model updating procedure followed in this work is based on a surrogate-based iterative method based on rEGO, which aims at minimising the Modified Total Modal Assurance Criterion (MTMAC) [36] to match the discretised FEM modal response to experimental results. The rEGO is preferred over classical EGO as it provides superior computational efficiency, robustness, and precision [3]. Nevertheless, any other iterative FEMU technique could be implemented with the same concept.

The expected contribution of the work is to prove that the proposed method is more computationally efficient when compared to the classical approach. Thus, the aim of this work is threefold:

- (i) Propose and assess the merits of the assembly-like approach;
- (ii) Employ the rEGO-based FEMU technique on a real complex structure;
- (iii) Obtain an updated discretised FEM of the structure.

## 2. The Refined Efficient Global Optimisation for Model Updating

rEGO [5, 3] was introduced to broaden the search capability of the Efficient Global Optimization (EGO) [37, 38]. The main aim was to establish rEGO as a global-local technique, in a hybrid sense [39], able to both navigate search spaces globally (avoiding local minima) and land, not only, in the area of the global minimum but as close as possible to it, via the implementation of refinement and selection techniques. The main novelties of EGO were the use of a Kriging surrogate model and the implementation of a new infill metric, the expected improvement (EI). The EI can be defined as a measure of how much could the known minimum improve if a given point was added to the data pool. The EGO workflow is similar to other surrogate-based techniques: (i) the design space is searched strategically, usually with Latin hypercube sampling [40], (ii) the absolute value of the EI is maximised to find the suitable infill point and (iii) the point is infilled. The process is iterated between (ii) and (iii) until convergence is reached. For EGO, usually, this happens when EI is less than 1% of the objective function minimum [37]. In order to improve this process, rEGO retains the same global structure but introduces two important principles: refinement and selection.

In this work, rEGO is considered due to its superior computational performance when compared to GAs and EGO [5, 3]. This means that a Kriging function, the same as per EGO, is used in this work as the surrogate model for the optimisation problem. A suitable objective function for FEMU via rEGO was identified in [5] in the MTMAC, which compares the experimental and numerical modal data,  $\omega_n$  and MAC values, thus  $\phi_n$ . The MTMAC was proven in [5] to outperform, computationally and precision-wise, other goal functions commonly used for FEMU. Hence, the residuals product of the MTMAC is used in this work and its formulation is presented as:

$$\text{MTMAC} = 1 - \prod_{i=1}^n \frac{\text{MAC}(\phi_i^E, \phi_i^N)}{\left(1 + \frac{|\omega_i^N - \omega_i^E|}{|\omega_i^N + \omega_i^E|}\right)} \quad (1)$$

where  $n$  denotes the number of modes, superscript E for experimental data and superscript N for numerical data.

In this work, the minimisation of the MTMAC for FEMU is based on the tuning of the structure's physical and geometrical properties. This is discussed in depth in later sections.

The reader interested in a more thorough review of EGO is referred to [37, 40, 38] and to [5, 3] for the introductory work on rEGO. A MATLAB tutorial for rEGO can be found in [41].

### 3. The Flexible Wing Model

The wing model chosen to validate the FEMU technique is a high aspect ratio (HAR) flexible wing model developed at Cranfield University for the Beam Reduction Dynamic Scaling (BeaRDS) project [42, 43, 44, 45]. The main aim of BeaRDS was to establish a workflow for the design, manufacture and testing of dynamically scaled HAR wings for use in Cranfield University 8×6 ft (2.4×1.8 m) wind tunnel. Specifically, the wing under scrutiny is the eXperimental BeaRDS-2 (XB-2) model (Figure 1a); a dynamically scaled model for an optimised (drag reduction) wing to be used in an A320-like aircraft. The scaled model is made up of four main components: the spar, the stiffening tube, the additional brass ballasts and the skin. The spar and stiffening tube serve as the wing torque box (Figure 1b), the brass ballasts were added for dynamic scaling purposes [47] and the skin was designed to minimise its effect on the wing stiffness [43]. Since dynamic scaling is not the focus of this work, the brass ballasts are removed for the current study. The spar is machined from two 6082-T6 Aluminium Alloy blocks and joined at mid-span with a weld and reinforced by four bolted L-section plates. Geometrically the spar can be divided into three main sections, according to its profile, as shown in Figure 1a. The spar mass is 1.225 kg.

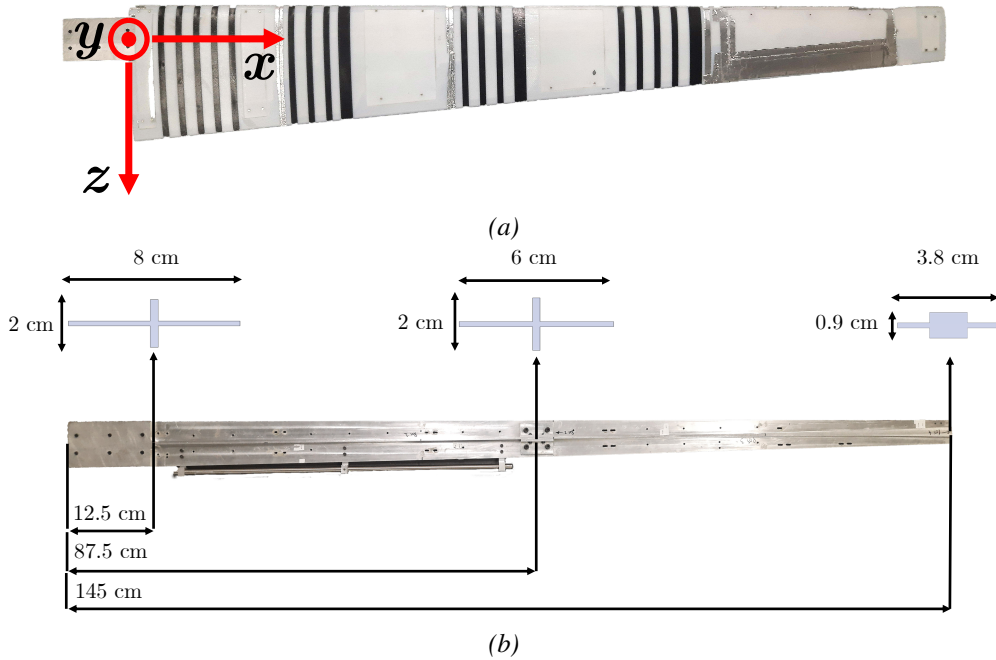


Figure 1: XB-2: Top views of the full wing (Figure 1a - axes reference system for the  $\phi_n$  plot (Adapted from [48])) and the torque box (Figure 1b - Adapted from [46]). Figure 1b also features the spar cross-sections and information about their span-wise position. Not in scale.

A stiffening tube was added aft of the spar to postpone flutter onset during the wind tunnel test of the BeaRDS project [47]. The tube is linked to the main spar at three points (near each end and in the middle), as shown in Figure 1a. The tube is made of stainless steel and features an outer diameter of 10 mm, with a thickness of 1 mm and a length of 600 mm. The torque box, consisting of the spar and the tube assembly, has a combined mass of 1.362 kg.

The outer surface of the wing is defined by the skin (Figure 1a), made up of 47 different subsections, which are 3D printed in Digital ABS (white) and Agilus 30 (black), a rubber-like material. Despite the use of different materials for the adjacent strips, the skin is made only of three separate parts, thanks to the PolyJet technology, which allows for the 3D printing of subsequent layers with different materials [49]. This, and the use of a rubber-like material, gives enhanced flexibility to the wing skin, allowing for large tip displacements. The assembly of the torque box and the skin constitutes the full wing. Table 1 introduces the wing material and physical properties, including aerofoil, aspect

ratio (AR), mean aerodynamic chord ( $\bar{c}$ ), taper ratio ( $\lambda$ ), Leading Edge sweep ( $\Lambda_{LE}$ ) and quarter-chord sweep ( $\Lambda_{c/4}$ ). Please note, the wing has a neutral twist and dihedral angles.

Table 1: Materials and physical properties.

Material	E - Young Modulus [GPa]	Poisson Ratio [-]	$\rho$ - Density [kgm] <sup>-3</sup>
6082-T6 Aluminium	70	0.33	2700
Stainless Steel	193	0.33	8000
Digital ABS	2.6–3.0	0.33 [50]	1170–1180
Agilus 30	3e-3 [51]	0.40 [52]	1140

Property	Details	Unit
Semi span	1.5	m
AR	18.8	-
$\bar{c}$	172	mm
$\lambda$	0.35	-
$\Lambda_{LE}$	14.9	°
$\Lambda_{c/4}$	0	°
Aerofoil	NACA 23015	-
Mass	3.024	kg

The reader interested a more profound review of the BearDS project is referred to [42, 43, 44, 45, 47] and further information on the XB-2 wing can be found in [43, 45, 34, 53].

### 3.1. Preliminary Finite Element Models

Having outlined the general geometry, components and properties of the XB-2, three preliminary discretised FEMs are built in ANSYS Mechanical APDL 2021. Respectively, a spar, torque box and full wing are built following an assembly-like approach. First, the spar model is built, then the tube is added for the torque box model and finally, the wing skin is modelled. This approach can be followed because experimental data of each scenario is available in [34].

The spar is easily discretised as a beam with 3 different portions. The first section is rectangular and represents the clamped root. Then three sections are defined along the spar to represent the three different section profile changes; hence, defining the two tapered sections along the span. The reinforcement plates are modelled as a 63 g lumped mass at mid-span. BEAM188 and MASS21 elements are used to, respectively, model the spar and the reinforcement plates. 6082-T6 Aluminium is assigned to the three sections. The BEAM188 element is based on Timoshenko beam theory with a first-order shear-deformation theory, while MASS21 element represents a single-node concentrated mass with components in the element coordinate directions. In Figure 2 (top), the FEM of the spar is shown with its boundary conditions. The constrained end of the spar is identified by the yellow arrows, while the plates, discretised as a lumped mass, are shown as a cyan asterisk.

Building on the spar model, the torque box FEM is constructed by adding the stiffening tube aft of the existing spar. The tube is discretised with a BEAM188 element and it is linked to the spar with 3 rigid link constraints (CERIG - rigid constraints between a master and slave node) for all degrees of freedom, shown in magenta in Figure 2 (middle). Stainless steel material properties are assigned to the tube.

Finally, the full wing model is created by adding the skin, as shown in Figure 2 (bottom). The skin is designed to limit the impact of the skin on the model overall stiffness [45]. This statement is verified numerically with solid-element FEMs of the skin and the torque-box assembly in ANSYS Workbench Mechanical. The two FEMs are used to obtain the tip deflection ( $\delta_{tip}$ ) from a static force input ( $P$ ) at the tip of 1 N. Then, by assuming the standard relationship from Euler–Bernoulli analysis of uniform cantilever beams:

$$\delta_{tip} = \frac{PL^3}{3EI} \Rightarrow EI = \frac{PL^3}{3\delta_{tip}} \quad (2)$$

the results in Table 2 are obtained, which prove that the bending stiffness,  $EI$ , of the skin is negligible if compared to that of the torque box, as the latter is only 1% of the former. Hence, the skin can be suitably discretised as lumped

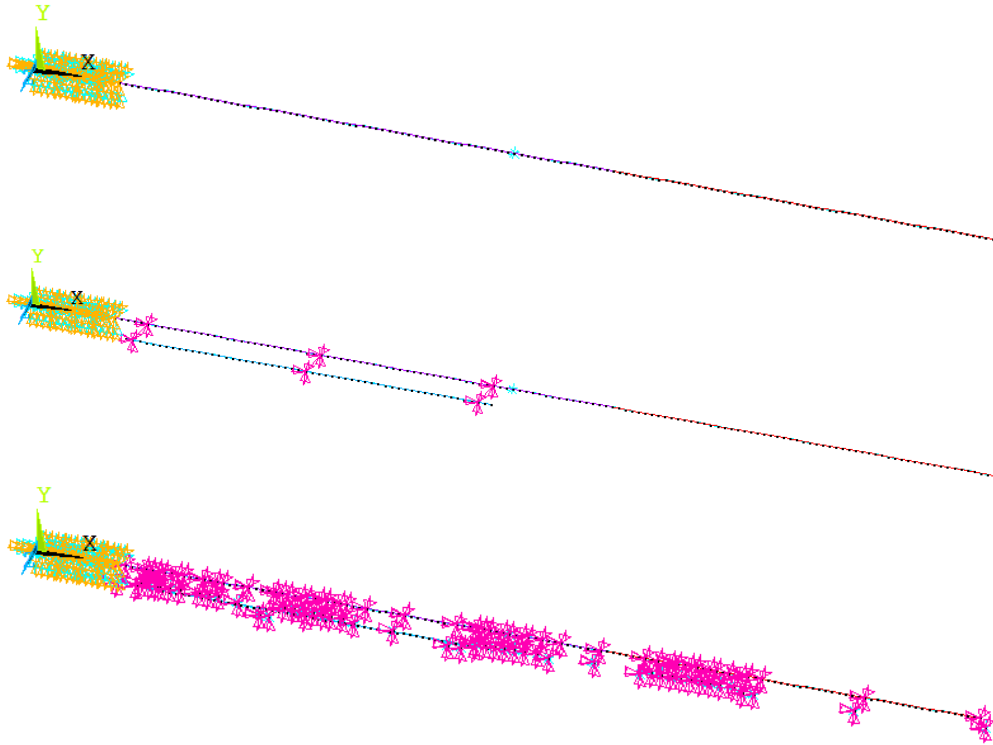


Figure 2: FEMs of the spar (top), torque box (middle) and full wing (bottom).



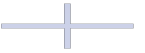


Table 2: Results of the static analyses in ANSYS Workbench Mechanical for the torque box and skin. Only the suspended lengths were considered, without the clamped root.

Quantity	Torque box	Skin
$P$ [N]	1	1
$L$ [m]	1.325	1.385
$\delta_{tip}$ [m]	4.7337e-3	0.51619
$EI$ [Nm <sup>2</sup> ]	163.8	1.72

masses, modelling each strip as a separate mass, since it does not bring any appreciable stiffening contribution due to the use of the Agilus 30 strips between the Digital ABS sections. Thus, forty-seven lumped masses are added to the model as MASS21 elements with CERIG links to the spar.

Table 3 shows properties of the sections of interest described above, including moments of inertia ( $I_{xx}$  and  $I_{yy}$ ) in m<sup>4</sup>, areas (A) in m<sup>2</sup> and torsion constants (J) in m<sup>4</sup>.

Table 3: Sections properties (Images not to scale).

Section					
$I_{xx}$ [m <sup>4</sup> ]	$5 \times 10^{-8}$	$6.50 \times 10^{-8}$	$3.46 \times 10^{-8}$	$1.29 \times 10^{-8}$	$1.68 \times 10^{-10}$
$I_{yy}$ [m <sup>4</sup> ]	$6.50 \times 10^{-7}$	$2.30 \times 10^{-9}$	$1.90 \times 10^{-9}$	$1.24 \times 10^{-9}$	$1.68 \times 10^{-10}$
A [m <sup>2</sup> ]	$14.60 \times 10^{-4}$	$2.07 \times 10^{-4}$	$1.69 \times 10^{-4}$	$1.98 \times 10^{-4}$	$1.49 \times 10^{-11}$
J [m <sup>4</sup> ]	$7 \times 10^{-7}$	$4.5 \times 10^{-10}$	$3.1 \times 10^{-10}$	$3 \times 10^{-9}$	$3.38 \times 10^{-10}$



The modal parameters are obtained from the FEMs by clamping the root of the specimens and running a damped modal analysis for extracting the modes between 0 and 150 Hz. Rayleigh damping is used for the definition of the damping coefficients, which were derived from the experimental results in [34]. Details are provided in the following sections. An element size of 0.001 m is set, as it is found not to condition results or adversely affect the computational efficiency.

### 3.2. Experimental Setup

In order to validate and, if needed, update the models, experimental data is needed. A previous testing campaign on the above-mentioned wings and sub-assemblies has been conducted in [34] and the results are used in this work.

A bandwidth-limited, between 2 and 400 Hz, random verification at 0.305 g RMS (root mean square) input is carried out for the spar, torque box, and full wing assemblies using a shaker table, resulting in an 18 min long signal. Eight accelerometers, distributed on four rows across the span are used to collect the vertical acceleration data, due to equipment constraints. Hence, only vertical displacements and rotation can be inspected. This is not a problem as we are focusing on the out-of-plane dynamics and the first in-plane mode is known to exist at around 16 Hz [34]. The modal parameters of the first three vertically dominant modes are then obtained via the industry-standard method [54] Least Squares Complex Exponential [55, 56].

The reader interested in the full experimental work, including details of the setup, acquisition system and post-processing, is referred to [34, 53] for further experimental work on XB-2.

### 3.3. Experimental Campaign and Preliminary Finite Element Models Results

This subsection reports on the modal parameters extracted from the preliminary FEMs and compares them with those from the GVT campaign in [34].

In Table 4, the  $\omega_n$  of from the experimental campaign are compared with those found from the damped modal analysis in Ansys Mechanical APDL 2021 R1, while only the  $\zeta_n$  identified from the experimental campaign are shown. As usual, bending refers to modes with a predominant vertical (y-axis) displacement and lagging with a predominant horizontal (z-axis) displacement. The coupled modes considered in this study are coupled between bending and torsion (around the x-axis).

Table 4: Natural frequencies identified from the experimental data and the preliminary FEMs.

Natural Frequencies [Hz]								
Mode	Spar		Torque box			XB-2 wing		
	Exp.	FEM (%)	Mode	Exp.	FEM (%)	Mode	Exp.	FEM (%)
1 <sup>st</sup> Bending	4.855	5.447 (12.19)	1 <sup>st</sup> Bending	5.252	5.887 (12.10)	1 <sup>st</sup> Bending	3.187	3.539 (11.03)
1 <sup>st</sup> Lagging	-	26.917	2 <sup>nd</sup> Bending	25.933	30.617 (18.07)	1 <sup>st</sup> Coupled	11.752	-
2 <sup>nd</sup> Bending	26.966	30.597 (13.46)	1 <sup>st</sup> Lagging	-	35.080	2 <sup>nd</sup> Coupled	17.447	17.774 (1.88)
1 <sup>st</sup> Torsion	-	68.049	1 <sup>st</sup> Coupled	76.242	85.162 (11.70)	-	-	-
3 <sup>rd</sup> Bending	76.851	88.757 (15.49)	-	-	-	-	-	-
Damping Ratios [-]								
Mode	Spar		Torque box			XB-2 wing		
	Exp.	FEM	Mode	Exp.	FEM	Mode	Exp.	FEM
1 <sup>st</sup> Bending	0.033	-	1 <sup>st</sup> Bending	0.022	-	1 <sup>st</sup> Bending	0.024	-
2 <sup>nd</sup> Bending	0.010	-	2 <sup>nd</sup> Bending	0.014	-	1 <sup>st</sup> Coupled	0.047	-
3 <sup>rd</sup> Bending	0.014	-	1 <sup>st</sup> Coupled	0.017	-	2 <sup>nd</sup> Coupled	0.038	-

Notably, more modes are, generally, identified in the same frequency interval in the FEMs. Table 4 shows only the results for the modes identified between the first and last modes that can be found in both the experimental and FEMs



data. At least three coincident modes are found for the spar (the first three bending modes) and torque box (the first bending and the first two coupled modes); however, this is not the case for the full wing. Only two coherent modes are identified and, thus, they are used for the FEMU process. Hence, three modes are considered for the FEMU of the spar and torque box, while only two for the FEMU of the full wing.

The  $\zeta_n$  values shown in Table 4 were found to obey classical Rayleigh damping. Hence, Rayleigh damping was assumed in the FEMs and the relative  $\alpha$  and  $\beta$  parameters were obtained by fitting the formulation below.

$$\mathbf{C} = \alpha \mathbf{M} + \beta \mathbf{K} \quad \text{and} \quad \zeta = \frac{1}{2} \left( \frac{\alpha}{\omega} + \beta \omega \right) \quad (3)$$

where  $\mathbf{C}$  is the damping matrix,  $\alpha$  is the mass proportional Rayleigh damping coefficient,  $\beta$  is the stiffness proportional Rayleigh damping coefficient,  $\mathbf{M}$  is the mass matrix,  $\zeta$  is the damping ratio and  $\omega$  is the frequency in  $\text{rads}^{-1}$ . In terms of  $\phi_n$ , the MAC values between the experimental and FEM results are above 0.9, except for the 1<sup>st</sup> coupled mode of the torque box and the 2<sup>nd</sup> coupled mode of the full wing. They stand at 0.8 and 0.75 respectively.

Given the results outlined for the preliminary FEMs, the FEMU task is fundamental to guarantee a model that represents as closely as possible the real system. Particular attention should be paid to the parameters that are furthest from the experimental values, such as the above-mentioned  $\phi_n$  and most of the  $\omega_n$ .

#### 4. Finite Element Model Updating of the Flexible Wing

The FEMU procedure follows a standard approach for surrogate-based iterative FEMU methods. In this section, the practical implementation of the point infill when  $\max(\text{EI})$  is reached in the MATLAB-based rEGO (as available in [41]) and the Ansys Mechanical APDL model.

First, a baseline discretised FEM is defined as an input file for Ansys Mechanical APDL. The input file takes some parameters, linked to the model properties. The MATLAB implementation finds the set of parameters from rEGO and modifies the input file accordingly, then, still within MATLAB, ANSYS Mechanical APDL is called to run the input file. After this is completed, another file, with the modal parameters results from the FEM, is generated from ANSYS and imported into MATLAB to calculate the MTMAC and recompute the surrogate model. This is shown in Figure 3a, while, for a practical implementation, the interested reader can refer to the [Data Availability Statement](#).

##### 4.1. Updating Parameters and the Assembly-like Approach

A set of parameters needs to be defined to carry out the FEMU process. Modal properties are a direct function of material and geometric properties in discretised models. Hence, their tuning is considered in this work for the FEMU task. The density  $\rho$  of all materials, as per Table 1, is selected as an updating parameter. The same is done for the Young Modulus  $E$  of all materials, apart from the Agilus 30 and the Digital ABS, because the skin is modelled as lumped masses (no stiffness). In addition, the geometric properties, such as  $I_{yy}$  and  $J$ , are selected as optimisation variables. The lumped mass used to model the reinforcement plates at the spar mid-span is employed as updating parameters. Lastly, a conceptual FEMU on the spar showed that the FEM would not converge adequately to the experimental results using only one material definition. Hence, the two halves of the spar are defined with two different material entries with base values for 6082-T6 aluminium.

A total of fifteen parameters are identified across all the specimens for the FEMU process. For the assembly-like approach, the parameters are assigned to a given part or sub-assembly. For the spar FEMU, eight parameters are updated, while for the torque box thirteen and for the XB-2 model all fifteen are tuned. The parameters specific to the spar model include the two 6082-T6 Aluminium densities and  $E$ , the reinforcement plates lumped mass, and the  $I_{yy}$  of the three spar sections ( $x_{1-4,9,10,12,14}$ ). The torque box includes all those from the spar and adds, the  $\rho$  and  $E$  for the stainless steel tube and the  $J$  of the three spar sections ( $x_{7,8,11,13,15}$ ). Finally, the XB-2 wing inherits all the parameters from the torque box plus those relative to the modelling of the skin as lumped masses ( $x_{4,5}$ ): the densities of Agilus 30 and Digital ABS. The updating parameters lower and upper bounds ratios are set at 0.6 and 1.4 and they actively scale the baseline value to match the FEM response to the experimental one. See Table 5 for a breakdown of the variables to be updated and Figure 3b for a workflow of the model updating and data fetching.

Since the main aim of this work is to investigate the goodness and feasibility of the assembly-like approach for the FEMU of complex structures, different updating scenarios have to be defined. Two approaches are determined. The

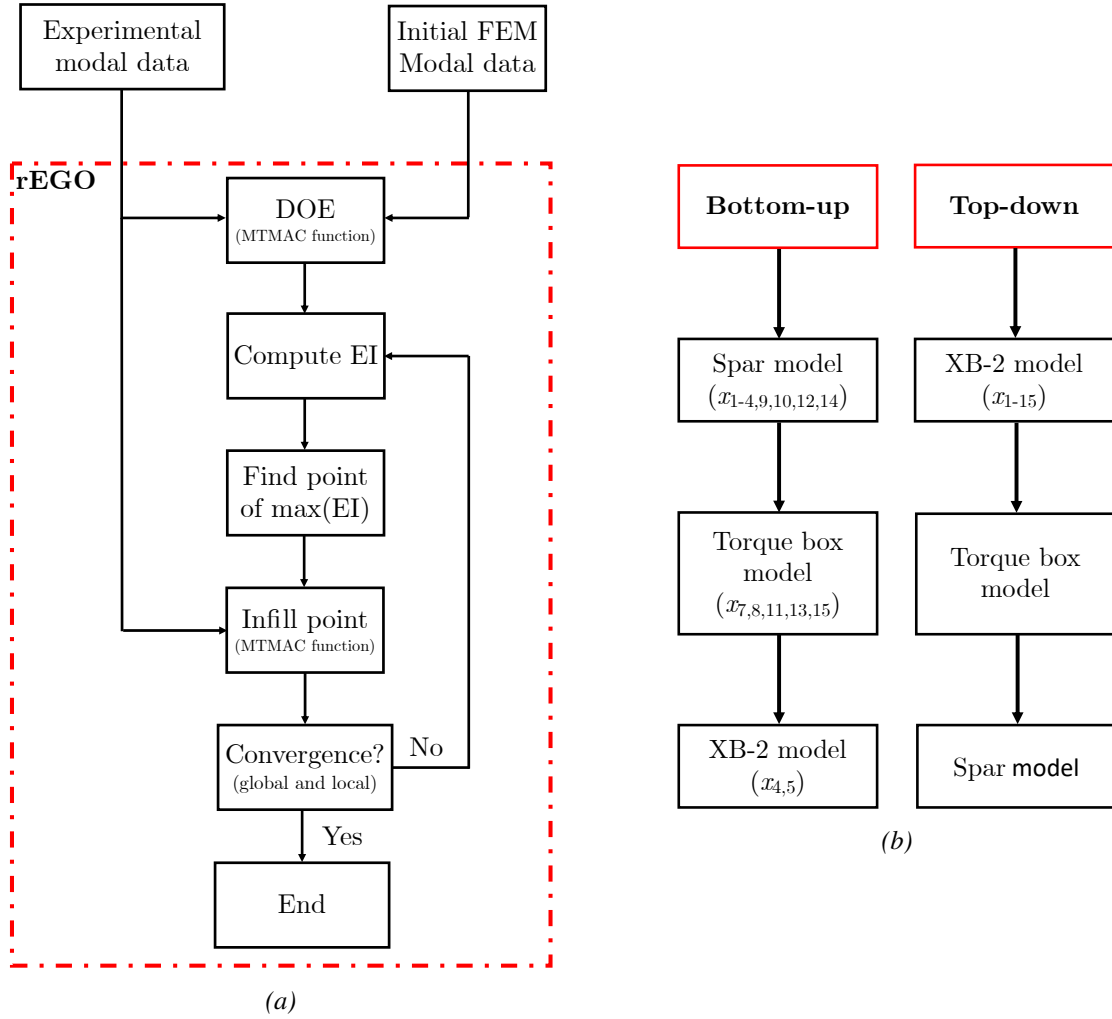


Figure 3: FEMU workflow: Figure 3a shows the optimisation workflow (in the red box the rEGO implementation) and Figure 3b the assembly-like structure and relative optimisation variables.

first considers the spar FEM as the base for the assembly-like approach and the torque box and XB-2 wing models are built from there. This, known as the bottom-up approach, means that the spar model is first updated, and then FEMU is carried out on the torque box and the wing, by carrying over the parameters updated in the previous component. On the other hand, the traditional approach works the other way around, as a top-down approach. First, the XB-2 wing model is updated taking into consideration all fifteen parameters and the torque box and spar model are built with the fetched parameters identified in that study. Table 6 and Figure 3b recap the phases of the assembly-like approach.

#### 4.2. The Spar

First, let us consider the results in terms of  $\omega_n$  for the spar. In Table 7 the  $\omega_n$  obtained from the experimental campaign (Exp.), preliminary FEM (FEM), FEM updated via bottom-up (FEMU\_1) and FEM updated via top-down (FEMU\_2) are compared.

The results for the bottom-up approach are good, in terms of  $\omega_n$  identification. The bottom-up approach provides the best performance, while the top-down approach proves to be the less accurate method in this instance. The top-down approach  $\omega_n$  are higher than those identified by the preliminary FEM, apart from the first bending mode.

The analysis on the identified  $\phi_n$  is presented in Figure 4 and Table 7. The  $\phi_n$  from the experimental data, preliminary FEM and updated FEMs are superimposed for comparison in Figure 4, which is further investigated in

Table 5: Properties updated for the FEMU processes.

	<b>Property</b>	<b>Description</b>	<b>Model</b>
$x_1$	6082-T6 aluminium $\rho$	$\rho$ of the inboard half of the spar.	Spar
$x_2$	6082-T6 aluminium E	E of the inboard half of the spar.	Spar
$x_3$	6082-T6 aluminium $\rho$	$\rho$ of the outboard half of the spar.	Spar
$x_4$	6082-T6 aluminium E	E of the outboard half of the spar.	Spar
$x_5$	Digital ABS $\rho$	$\rho$ of the Digital ABS sections.	XB-2 wing
$x_6$	Agilus 30 $\rho$	$\rho$ of the Agilus 30 sections.	XB-2 wing
$x_7$	Stainless steel $\rho$	$\rho$ of the stainless steel tube.	Torque box
$x_8$	Stainless steel E	E of the stainless steel tube.	Torque box
$x_9$	Reinforcement plates	Lumped mass value for the reinforcement plates discretisation.	Spar
$x_{10}$	$I_{yy}$ spar (inboard)	Spar inboard cross-section $I_{yy}$	Spar
$x_{11}$	J spar (inboard)	Spar inboard cross-section J	Torque box
$x_{12}$	$I_{yy}$ spar (inboard)	Spar mid-span cross-section $I_{yy}$	Spar
$x_{13}$	J spar (inboard)	Spar mid-span cross-section J	Torque box
$x_{14}$	$I_{yy}$ spar (inboard)	Spar outboard cross-section $I_{yy}$	Spar
$x_{15}$	J spar (inboard)	Spar outboard cross-section J	Torque box

Table 6: Assembly-like approach schematic.

<b>Assembly-like Approach</b>		
	Bottom-up (FEMU_1)	Top-down (FEMU_2)
Spar	FEMU - 8 parameters	Fetching 8 parameters
Torque box	FEMU - 5 parameters	Fetching 13 parameters
XB-2 wing	FEMU - 2 parameters	FEMU - 15 parameters

Table 7: Natural frequencies identified from the experimental data, the preliminary FEM and the updated FEMs for the spar. MAC values (diagonal terms only) of the models wrt the experimental data.

<b>Natural Frequencies [Hz]</b>				
<b>Mode</b>	Exp.	FEM (%)	FEMU - Bottom-up (%)	FEMU - Top-down (%)
1 <sup>st</sup> Bending	4.885	5.447 (12.19)	4.855 (-)	5.062 (4.26)
2 <sup>nd</sup> Bending	26.966	30.597 (13.46)	26.864 (-0.38)	31.775 (17.83)
3 <sup>rd</sup> Bending	76.851	88.757 (15.49)	80.624 (4.91)	95.269 (23.97)
<b>MAC Values (of the diagonal) [-]</b>				
<b>Mode</b>	FEM	FEMU - Bottom-up (%)	FEMU - Top-down (%)	
1 <sup>st</sup> Bending	0.98	0.99	0.99	
2 <sup>nd</sup> Bending	0.94	0.98	0.97	
3 <sup>rd</sup> Bending	0.90	0.98	0.94	

Table 7. There, the diagonal values of the MAC matrix are presented. Please note, the off-diagonal terms are not shown due to their negligible magnitude.

Globally, all FEMs offer a good approximation of the spar  $\phi_n$  showing numerical correlation with values above 0.94 in Table 7 and graphical correlation in Figure 4. Nevertheless, the bottom-up approach performs better than the top-down approach and it is a clear improvement over the preliminary FEM. Notably, all the modes identified from the top-down approach are well correlated to the experimental case; however, they show less improvement than the bottom-up approach.

In order to compare the  $\omega_n$  and  $\phi_n$  together, the penalty function of the optimisation routine can be considered,

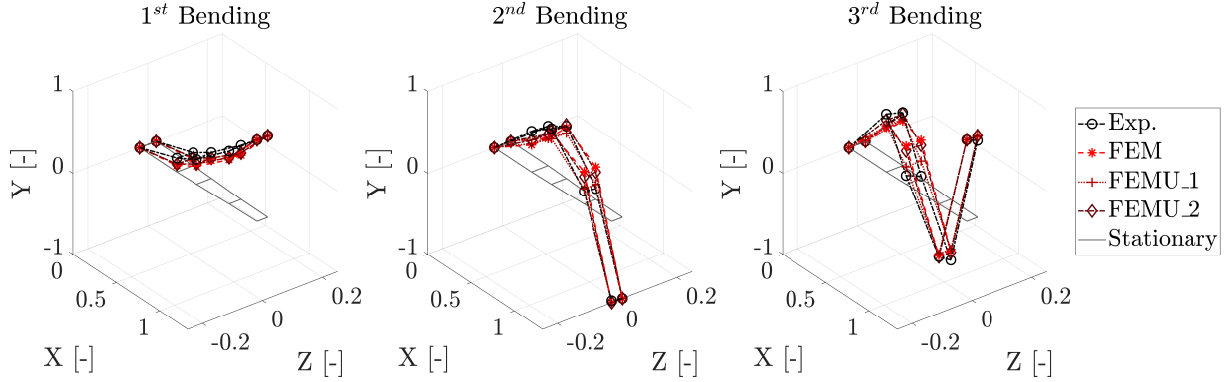


Figure 4: Mode shapes identified from the experimental data (Exp.), the preliminary FEM (FEM) and the updated FEMs (FEMU\_1-2) for the spar.

the MTMAC. The MTMAC for the preliminary FEM is 0.30, for bottom-up is 0.07 and for top-down is 0.26. Clearly, bottom-up, globally, shows an improvement over the preliminary FEM. This means that the small deterioration in the  $\omega_n$  is counterbalanced by a greater precision in the  $\phi_n$  identification. In terms of computational power, the top-down FEM takes the parameters from the FEMU of the XB-2 wing. However, bottom-up FEMU is carried out on the spar itself. The rEGO needs 327 model evaluations to converge to the presented results for the bottom-up approach.

#### 4.3. The Torque Box

The  $\omega_n$  identified for the torque box from the updated FEMs are compared to those from experimental data and the preliminary FEM in Table 8.

Table 8: Natural frequencies identified from the experimental data, the preliminary FEM and the updated FEMs for the torque box. MAC values (diagonal terms only) of the models wrt the experimental data.

Mode	Natural Frequencies [Hz]			
	Exp.	FEM (%)	FEMU - Bottom-up (%)	FEMU - Top-down (%)
1 <sup>st</sup> Bending	5.252	5.887 (2.76)	5.658 (7.73)	5.354 (1.94)
2 <sup>nd</sup> Bending	25.933	31.452 (21.18)	32.663 (25.95)	31.092 (19.89)
1 <sup>st</sup> Coupled	76.242	86.344 (13.25)	82.992 (8.85)	68.926 (-9.60)
Mode	MAC Values (of the diagonal) [-]			
	FEM	FEMU - Bottom-up	FEMU - Top-down	
1 <sup>st</sup> Bending	0.99	0.99	0.99	
2 <sup>nd</sup> Bending	0.96	0.95	0.96	
1 <sup>st</sup> Coupled	0.83	0.84	0.76	

The  $\omega_n$  identified from the preliminary FEM seems to be more closely related to those from experimental data. Their maximum error is 21.18%, which is less than the maximum error for the bottom-up FEM. Notably, the maximum errors are always found for the second bending mode. On the other hand, the FEM from top-down has the lowest error (1.94%) for  $\omega_1$ . This is a small improvement over the preliminary FEM, but it is much better than the bottom-up FEM (7.73%). Until now, all the FEM approaches have overestimated the  $\omega_n$  values. However, this changes with the first coupled mode identified by the top-down approach for the torque box, which underestimates the experimental value by 9.6%. Concerning  $\omega_3$ , the bottom-up FEM shows an improvement over the preliminary FEM value, but the values for the other modes are overestimated. As it is clear from Table 8, no model can be clearly set as the best, in terms of  $\omega_n$  identification for the torque box.

From Figure 5, it is clear that the most problematic  $\phi_n$  to identify is the first coupled mode. In particular, it seems that the FEMs struggle to mimic the amplitude of the torsional rotation. This affects on the MAC values, since the lowest values are found for the first coupled mode, where the highest value is 0.84 for the bottom-up updated FEM. In

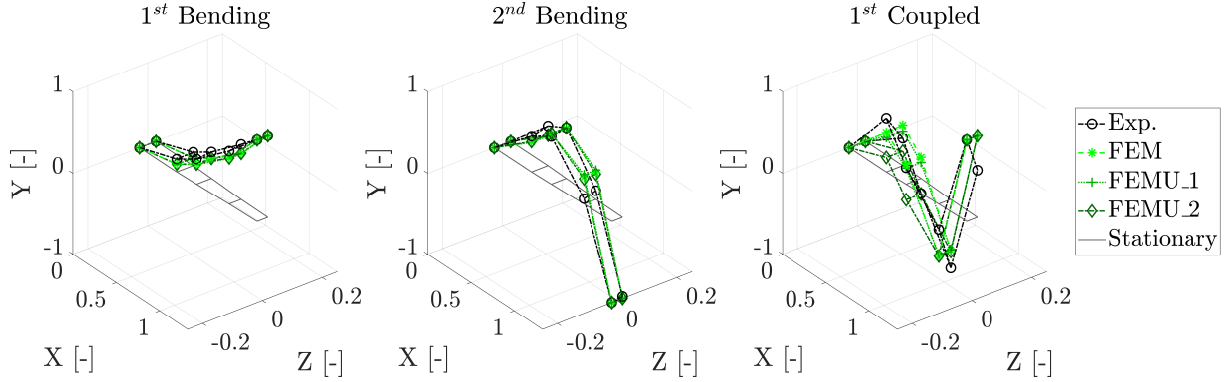


Figure 5: Mode shapes identified from the experimental data (Exp.), the preliminary FEM (FEM) and the updated FEMs (FEMU\_1-2) for the torque box.

terms of MAC values, the preliminary FEM and the bottom-up FEM perform similarly. The same could be said about the top-down FEM, but the last mode results are not satisfactory.

In order to consider  $\omega_n$  and  $\phi_n$  simultaneously, the MTMAC values with respect to the experimental data should be examined. The preliminary FEM MTMAC value is 0.34, that of bottom-up FEM is 0.35 and for top-down FEM is 0.37. Higher values of the MTMAC for the updated FEMs are unexpected. This has to do with the nature of the discretisation, mainly focused on out-of-plane dynamics rather than twisting motions, which first appear for the torque box model. The bottom-up model performs better than the top-down model, but still not as well as the preliminary model. In terms of model evaluations to convergence, the bottom-up model took 780 evaluations to be updated starting from the spar model.

#### 4.4. The XB-2 wing

Table 9 gives a quantitative overview of the precision, relative to the experimental data, of the parameters extracted via the FEMs. All FEM-extracted parameters are very close to the experimental data. The maximum error, relative to the experimental  $\omega_n$ , for the updated FEMs is 0.01% in the bottom-up FEMU.

Table 9: Natural frequencies identified from the experimental data, the preliminary FEMs and the updated FEM for the XB-2 wing. MAC values (diagonal terms only) of the models wrt the experimental data.

Natural Frequencies [Hz]				
Mode	Exp.	FEM (%)	FEMU - Bottom-up (%)	FEMU - Top-down (%)
1 <sup>st</sup> Bending	3.187	3.5397 (11.03)	3.187 (-)	3.187 (-)
2 <sup>nd</sup> Coupled	17.447	17.774 (1.88)	17.448 (0.01)	17.447 (-)
MAC Values (of the diagonal) [-]				
Mode	FEM	(%)	FEMU - Bottom-up (%)	FEMU - Top-down (%)
1 <sup>st</sup> Bending	0.98	0.99	0.99	0.99
2 <sup>nd</sup> Coupled	0.75	0.77	0.77	0.78

In Figure 6 the first  $\phi_n$  is almost a perfect overlap for all FEMs. However, this does not happen for the second coupled mode, where, despite following the vertical deflection, the torsional magnitude is much smaller. These are confirmed in the quantitative analysis in Table 9, where the MAC values for the first bending mode are close to 1 for the updated FEMs and 0.98 for the preliminary model, but those for the second coupled mode do not go over 0.78, stopping at 0.75 for the preliminary FEM and 0.77 for the bottom-up FEM. This has to be redirected to the nature of discretisation, which is focused on the out-of-plane dynamics.

In order to give equal consideration to  $\omega_n$  and  $\phi_n$  the MTMAC is addressed. The starting MTMAC for the XB-2 wing is 0.30, but the updated models are able to reduce to 0.24 (bottom-up) and 0.23 (top-down). In terms of

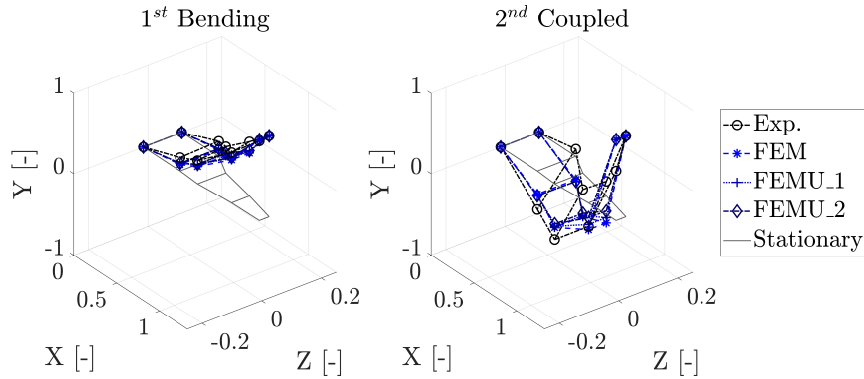


Figure 6: Mode shapes identified from the experimental data (Exp.), the preliminary FEM (FEM) and the updated FEMs (FEMU\_1-2) for the XB-2 wing.

percentages, the MTMAC of the bottom-up approach improved by 20%, while the top-down approach improved by 23%. Similar results in terms of precision are delivered by the bottom-up and 2 updated FEMs; however, the use of computational power needs to be taken into account. The top-down optimisation over 15 parameters took 1462 evaluations, all on the XB-2 wing model, excluding any top-down iterations for the torque box or the spar models alone. On the other hand to obtain a relevant number the evaluations of all preceding models need to be accounted for. The spar model took 327 evaluations to converge, the torque box model converged after 780 evaluations and, lastly, the final update took 57 evaluations, totalling 1164. It should be noted that the most computationally expensive model (the full wing) is evaluated only 54 times in the bottom-up approach, while, by definition, it is evaluated 1462 in the top-down approach. This shows that the newly proposed bottom-up approach has a similar precision to the traditional approach with a lower computational burden.

In terms of model mass, the assembly-like method, as shown in Table 10, improves the mass matching of the initial FEM, even if this was not the main objective of the optimisation (although  $\rho$  is considered as a variable). On the other hand, the top-down FEM outperforms the two, at the cost of computational resources. However, this is a superficial analysis. It might seem that the top-down FEM is much better than the bottom-up FEM. However, this is not the case. In fact, when the actual and model masses for the torque box and skin are compared separately, the absolute errors (on the components) are similar for the two methods, with the newly proposed approach showing slightly better performance for the skin mass (6.80 vs 6.98%). These small (less than 8.5%) differences are to be attributed to the massless discretisation of the spar-to-tube links and to the uncertainty of the 3D-printed plastics density. Furthermore, they are sufficiently small and distributed (the errors absolute values for the torque box and skin in the two approaches are similar), which do not constitute a problem for potential further aeroelastic analyses and are a clear improvement wrt the initial model. Nevertheless, it is important to consider that the models developed here are discredited FEMs, such that the priority is to match the real system dynamics rather than the exact stiffness and mass values [17].

Table 10: Identified model masses.

Model of XB-2	Mass [kg] (relative error wrt experimental - %)		
	Torque box	Skin	Total
Experimental	1.362	1.662	3.024
Initial FEM	1.224 (-10.13)	1.458 (-12.27)	2.682 (-11.31)
Top-down FEM	1.250 (-8.22)	1.778 (+6.98)	3.029 (+0.02)
Bottom-up FEM	1.250 (-8.22)	1.549 (-6.80)	2.799 (-7.44)

These results highlight the computational advantage of the proposed assembly-like method and support the authors' claims that a paradigm shift towards assembly-like methods needs to be considered in FEMU. On the other hand, this approach might not be suitable for non-assemblable structures, such as buildings (although, some new con-

struction techniques could be considered to be assemblies and should be investigated). Nevertheless, other applicable examples suitable for assembly-like approaches could be small satellites, such as CubeSats, and other mechanical systems, such as aero-engines. However, complications might arise for systems that require altering the experimental setup to test their sub-components

## 5. Conclusions

In this work, a flexible wing finite element model is characterised and updated using modal data from an experimental campaign following two assembly-like, bottom-up and top-down, approaches. The main findings of this study can be condensed into the following points:


- A framework for assembly-like finite element model updating is proposed and applied to a flexible wing;
- The direct approach (top-down) and the assembly-like approach (bottom-up) have similar precision in modelling the flexible wing (3% difference in MTMAC and similar model mass estimation precision);
- The bottom-up approach is much more computationally efficient. It takes 20% less iterations to obtain convergence for the bottom-up approach;
- The top-down approach evaluates only the more expensive model of the full wing, while the bottom-up model has only 57, out of 1164, evaluations of the full wing model;
- To the authors' knowledge this is the first time that refined Efficient Global Optimisation is applied to a complex structure finite element model updating;
- It is the first updated finite element model available in the literature for the benchmark wing

Thus, the findings of this work support the paradigm shift of finite element model updating towards assembly-like approaches, which is the recommended approach for similar structures.

### Corresponding Author

Gabriele Dessena  - Corresponding author

E-mail address: [GDessena@ing.uc3m.es](mailto:GDessena@ing.uc3m.es)

James F. Whidborne  - Primary corresponding author

E-mail address: [J.F.Whidborne@cranfield.ac.uk](mailto:J.F.Whidborne@cranfield.ac.uk)

### Author Contributions

Conceptualisation, G.D.; methodology, G.D.; software, G.D.; validation, G.D.; formal analysis, G.D.; investigation, G.D.; resources, D.I., J.W., A.P., and L.Z.; data curation, G.D.; writing—original draft preparation, G.D.; writing—review and editing, G.D., D.I., J.W. A.P., and L.Z.; visualisation, G.D.; supervision, D.I., J.W., A.P., and L.Z.; funding acquisition, L.Z..

### Declaration of conflicting interests

The author(s) declared no potential conflicts of interest with respect to the research, authorship, and/or publication of this article.

### Funding

The authors from Cranfield University disclosed receipt of the following financial support for the research, authorship, and/or publication of this article: This work was supported by the Engineering and Physical Sciences Research Council (EPSRC) [grant number 2277626].



## Data Availability Statement

Data supporting (ANSYS Mechanical APDL input files and MATLAB scripts) this study are openly available from the Zenodo repository at [<https://doi.org/10.5281/zenodo.14025503>] under the terms of [GNU General Public License (GPLv3)].

## References

- [1] Z. Cao, H. Wei, D. Liang, Z. Jia, J. Yao, D. Jiang, *A non-intrusive dynamic sensitivity-based substructure model updating method for nonlinear systems*, *International Journal of Mechanical Sciences* 248 (July 2022) (2023) 108218. doi:10.1016/j.ijmecsci.2023.108218. URL <https://linkinghub.elsevier.com/retrieve/pii/S0020740323001200>
- [2] N. F. Alkayem, M. Cao, Y. Zhang, M. Bayat, Z. Su, *Structural damage detection using finite element model updating with evolutionary algorithms: a survey*, *Neural Computing and Applications* 30 (2) (2018) 389–411. doi:10.1007/s00521-017-3284-1. URL <http://link.springer.com/10.1007/s00521-017-3284-1>
- [3] G. Dessena, D. I. Ignatyev, J. F. Whidborne, L. Zanotti Fragonara, *A Kriging Approach to Model Updating for Damage Detection*, in: P. Rizzo, A. Milazzo (Eds.), *EWSHM 2022 (LNCE 254)*, lecture no Edition, Springer, Singapore, 2023, Ch. 26, pp. 245–255. doi:10.1007/978-3-031-07258-1\_26. URL [https://link.springer.com/10.1007/978-3-031-07258-1\\_26](https://link.springer.com/10.1007/978-3-031-07258-1_26)
- [4] X. Yang, X. Guo, H. Ouyang, D. Li, *A kriging model based finite element model updating method for damage detection*, *Applied Sciences* 7 (10) (2017) 1039. doi:10.3390/app7101039. URL <http://www.mdpi.com/2076-3417/7/10/1039>
- [5] G. Dessena, D. I. Ignatyev, J. F. Whidborne, L. Zanotti Fragonara, *A global–local meta-modelling technique for model updating*, *Computer Methods in Applied Mechanics and Engineering* 418 (2024) 116511. doi:10.1016/j.cma.2023.116511. URL <https://linkinghub.elsevier.com/retrieve/pii/S0045782523006357>
- [6] J. Mottershead, M. Friswell, *Model Updating In Structural Dynamics: A Survey*, *Journal of Sound and Vibration* 167 (2) (1993) 347–375. doi:10.1006/jsvi.1993.1340. URL <https://linkinghub.elsevier.com/retrieve/pii/S0022460X83713404>
- [7] M. I. Friswell, J. E. Mottershead, *Finite Element Model Updating in Structural Dynamics*, Vol. 38 of *Solid Mechanics and its Applications*, Springer Netherlands, Dordrecht, 1995. doi:10.1007/978-94-015-8508-8. URL <http://link.springer.com/10.1007/978-94-015-8508-8>
- [8] T. Marwala, *Finite-element-model Updating Using Computational Intelligence Techniques*, Springer London, London, 2010. doi:10.1007/978-1-84996-323-7. URL <http://link.springer.com/10.1007/978-1-84996-323-7>
- [9] F. Shadan, F. Khoshnoudian, D. J. Inman, A. Esfandiari, *Experimental validation of a FRF-based model updating method*, *Journal of Vibration and Control* 24 (8) (2018) 1570–1583. doi:10.1177/1077546316664675. URL <http://journals.sagepub.com/doi/10.1177/1077546316664675>
- [10] F. Forouzes, H. Ahmadian, M. Navidbakhsh, *A 3D finite element model updating of spinal lumber segment applying experimental modal data and particle swarm optimization algorithm*, *Journal of Vibration and Control* 29 (19-20) (2023) 4673–4686. doi:10.1177/10775463221123202. URL <http://journals.sagepub.com/doi/10.1177/10775463221123202>
- [11] F. De Florio, *Airworthiness*, Elsevier, 2011. doi:10.1016/C2010-0-65567-2. URL <https://linkinghub.elsevier.com/retrieve/pii/C20100655672>
- [12] S. Malik, S. Ricci, L. Riccobene, *Aeroelastic analysis of a slender wing*, *CEAS Aeronautical Journal* 11 (4) (2020) 917–927. doi:10.1007/s13272-020-00459-6. URL <https://link.springer.com/10.1007/s13272-020-00459-6>
- [13] D. Di Leone, F. L. Balbo, A. De Gaspari, S. Ricci, *Model updating and aeroelastic correlation of a scaled wind tunnel model for active flutter suppression test*, *Aerospace* 8 (11) (2021). doi:10.3390/aerospace8110334. URL <https://www.mdpi.com/2226-4310/8/11/334>
- [14] M. Mihaila-Andres, P.-V. Rosu, C. Larco, M. Demsa, L. Constantin, R. Pahonie, *Preliminary design of aeroelastically tailored wing box structures with bend-twist coupling*, *ITM Web of Conferences* 24 (2019) 2010. doi:10.1051/itmconf/20192402010. URL <https://www.itm-conferences.org/10.1051/itmconf/20192402010>
- [15] Y. Wang, A. Wynn, R. Palacios, *Nonlinear Aeroelastic Control of Very Flexible Aircraft Using Model Updating*, *Journal of Aircraft* 55 (4) (2018) 1551–1563. doi:10.2514/1.C034684. URL <https://arc.aiaa.org/doi/10.2514/1.C034684>
- [16] C. Chiodi, G. Coppotelli, J. V. Covioli, *Identification of the static and dynamic numerical model of a jet aircraft wing from experimental tests*, in: *AIAA Scitech 2021 Forum*, no. January, American Institute of Aeronautics and Astronautics, Reston, Virginia, 2021, pp. 1–21. doi:10.2514/6.2021-1498. URL <https://arc.aiaa.org/doi/10.2514/6.2021-1498>
- [17] J. Ceardle, *Updating of jet trainer aircraft dynamic model to results of ground vibration test*, in: *33rd Congress of the International Council of the Aeronautical Sciences, ICAS 2022*, no. 2, International Council of the Aeronautical Sciences, Stockholm, Sweden, 2022, pp. 1–9. URL [https://www.icas.org/ICAS\\_ARCHIVE/ICAS2022/data/papers/ICAS2022\\_0044\\_paper.pdf](https://www.icas.org/ICAS_ARCHIVE/ICAS2022/data/papers/ICAS2022_0044_paper.pdf)
- [18] W. Wang, X. Zhang, D. Hu, D. Zhang, P. Allaire, *A novel none once per revolution blade tip timing based blade vibration parameters identification method*, *Chinese Journal of Aeronautics* 33 (7) (2020) 1953–1968. doi:10.1016/j.cja.2020.01.014. URL <https://linkinghub.elsevier.com/retrieve/pii/S1000936120300959>

- [19] G. Dessena, M. Civera, L. Zanotti Fragonara, D. I. Ignatyev, J. F. Whidborne, **A Loewner-Based System Identification and Structural Health Monitoring Approach for Mechanical Systems**, *Structural Control and Health Monitoring* 2023 (2023) 1–22. doi:10.1155/2023/1891062. URL <https://www.hindawi.com/journals/schm/2023/1891062/>
- [20] G. Dessena, M. Civera, D. I. Ignatyev, J. F. Whidborne, L. Zanotti Fragonara, B. Chiaia, **The Accuracy and Computational Efficiency of the Loewner Framework for the System Identification of Mechanical Systems**, *Aerospace* 10 (6) (2023) 571. doi:10.3390/aerospace10060571. URL <https://www.mdpi.com/2226-4310/10/6/571>
- [21] Z. R. Lu, D. Yang, L. Huang, L. Wang, **Covariance regression for operational modal analysis**, *JVC/Journal of Vibration and Control* 28 (11-12) (2022) 1295–1310. doi:10.1177/1077546321990144. URL <https://journals.sagepub.com/doi/abs/10.1177/1077546321990144>
- [22] Z. Cao, Q. Fei, D. Jiang, D. Zhang, H. Jin, R. Zhu, **Dynamic sensitivity-based finite element model updating for nonlinear structures using time-domain responses**, *International Journal of Mechanical Sciences* 184 (April) (2020) 105788. doi:10.1016/j.ijmecsci.2020.105788. URL <https://linkinghub.elsevier.com/retrieve/pii/S0020740319348635>
- [23] M. H. Jalali, D. G. Rideout, **Frequency-based decoupling and finite element model updating in vibration of cable–beam systems**, *Journal of Vibration and Control* 28 (11-12) (2022) 1520–1535. doi:10.1177/1077546321996936. URL <http://journals.sagepub.com/doi/10.1177/1077546321996936>
- [24] G. Coppotelli, F. D. Giandomenico, C. Groth, S. Porziani, A. Chiappa, M. E. Biancolini, **On the structural updating using operational responses of a realistic wing model: The ribes test article**, in: 8th IOMAC - International Operational Modal Analysis Conference, Proceedings, International Operational Modal Analysis Conference (IOMAC), Copenhagen Denmark, 2019, pp. 321–334. URL <https://www.iomac.info/iomac2019>
- [25] R. J. Allemang, D. L. Brown, **A correlation coefficient for modal vector analysis**, in: Proceedings of the 1st International Modal Analysis Conference, Union College, Schenectady, NY, 1982, pp. 110–116. URL <https://web.archive.org/web/20151018074821/http://sdr1.uc.edu/sdr1/referenceinfo/documents/papers/imac1982-mac.pdf>
- [26] S. M. O. Tavares, J. A. Ribeiro, B. A. Ribeiro, P. M. S. T. de Castro, **Aircraft Structural Design and Life-Cycle Assessment through Digital Twins**, *Designs* 8 (2) (2024) 29. doi:10.3390/designs8020029. URL <https://www.mdpi.com/2411-9660/8/2/29>
- [27] B. Sharqi, C. E. Cesnik, **Finite Element Model Updating for Very Flexible Wings**, in: AIAA SCITECH 2022 Forum, American Institute of Aeronautics and Astronautics, Reston, Virginia, 2022, pp. 1–23. doi:10.2514/6.2022-1185. URL <https://arc.aiaa.org/doi/10.2514/6.2022-1185>
- [28] B. Sharqi, C. E. S. Cesnik, **Finite Element Model Updating for Very Flexible Wings**, *Journal of Aircraft* 60 (2) (2023) 476–489. doi:10.2514/1.C036894. URL <https://arc.aiaa.org/doi/10.2514/1.C036894>
- [29] W. Zhao, N. Muthirevula, R. K. Kapania, A. Gupta, C. D. Regan, P. J. Seiler, **A Subcomponent-based Finite Element Model Updating for a Composite Flying-wing Aircraft**, in: AIAA Atmospheric Flight Mechanics Conference, no. January, American Institute of Aeronautics and Astronautics, Grapevine, Texas, 2017, p. 30. doi:10.2514/6.2017-1393. URL <https://arc.aiaa.org/doi/10.2514/6.2017-1393>
- [30] W. Zhao, A. Gupta, C. D. Regan, J. Miglani, R. K. Kapania, P. J. Seiler, **Component data assisted finite element model updating of composite flying-wing aircraft using multi-level optimization**, *Aerospace Science and Technology* 95 (2019) 105486. doi:10.1016/j.ast.2019.105486. URL <https://linkinghub.elsevier.com/retrieve/pii/S1270963819304572>
- [31] D. McCrum, M. Williams, **An overview of seismic hybrid testing of engineering structures**, *Engineering Structures* 118 (2016) 240–261. doi:10.1016/j.engstruct.2016.03.039. URL <https://linkinghub.elsevier.com/retrieve/pii/S0141029616300748>
- [32] C. Yang, X. Cai, Z. Lai, Y. Yuan, **Hybrid Test on a Simply Supported Bridge With High-Damping Rubber Bearings**, *Frontiers in Built Environment* 6 (September) (2020) 1–9. doi:10.3389/fbuil.2020.00141. URL <https://www.frontiersin.org/article/10.3389/fbuil.2020.00141/full>
- [33] J. Wilson, G. Manson, P. Gardner, R. J. Barthorpe, **Hierarchical verification and validation in a forward model-driven structural health monitoring strategy**, *Structural Health Monitoring* (nov 2023). doi:10.1177/14759217231206698. URL <http://journals.sagepub.com/doi/10.1177/14759217231206698>
- [34] G. Dessena, D. I. Ignatyev, J. F. Whidborne, A. Pontillo, L. Zanotti Fragonara, **Ground vibration testing of a flexible wing: A benchmark and case study**, *Aerospace* 9 (8) (2022) 438. doi:10.3390/aerospace9080438. URL <https://www.mdpi.com/2226-4310/9/8/438>
- [35] G. Dessena, **Data supporting: Ground Vibration Testing of a Flexible Wing: A Benchmark and Case Study** (2022). doi:10.17862/cranfield.rd.19077023. URL <https://dspace.lib.cranfield.ac.uk/handle/1826/22471>
- [36] R. Perera, R. Torres, **Structural Damage Detection via Modal Data with Genetic Algorithms**, *Journal of Structural Engineering* 132 (9) (2006) 1491–1501. doi:10.1061/(ASCE)0733-9445(2006)132:9(1491). URL [https://doi.org/10.1061/\(ASCE\)0733-9445\(2006\)132:9\(1491\)](https://doi.org/10.1061/(ASCE)0733-9445(2006)132:9(1491))
- [37] D. R. Jones, M. Schonlau, W. J. Welch, **Efficient global optimization of expensive black-box functions**, *Journal of Global Optimization* 13 (1998) 455–492. doi:10.1023/A:1008306431147. URL <https://link.springer.com/article/10.1023/A:1008306431147>
- [38] A. I. J. Forrester, A. Sobester, A. J. Keane, **Engineering Design via Surrogate Modelling**, Wiley, 2008. doi:10.1002/9780470770801. URL <https://onlinelibrary.wiley.com/doi/book/10.1002/9780470770801>

- [39] A. J. Keane, J. P. Scanlan, *Design search and optimization in aerospace engineering*, Philosophical Transactions of the Royal Society A: Mathematical, Physical and Engineering Sciences 365 (1859) (2007) 2501–2529. doi:10.1098/rsta.2007.2019. URL <https://royalsocietypublishing.org/doi/10.1098/rsta.2007.2019>
- [40] A. I. Forrester, A. Sóbester, A. J. Keane, *Multi-fidelity optimization via surrogate modelling*, Proceedings of the Royal Society A: Mathematical, Physical and Engineering Sciences 463 (2088) (2007) 3251–3269. doi:10.1098/rspa.2007.1900. URL <https://royalsocietypublishing.org/doi/10.1098/rspa.2007.1900>
- [41] G. Dessena, *rEGO - A tutorial on the rEGO for model updating* (2023). doi:10.5281/zenodo.8406030. URL <https://doi.org/10.5281/zenodo.8406030>
- [42] A. Pontillo, D. Hayes, G. X. Dussart, G. E. Lopez Matos, M. A. Carrizales, S. Y. Yusuf, M. M. Lone, *Flexible High Aspect Ratio Wing: Low Cost Experimental Model and Computational Framework*, in: 2018 AIAA Atmospheric Flight Mechanics Conference, American Institute of Aeronautics and Astronautics, Reston, Virginia, 2018, pp. 1–15. doi:10.2514/6.2018-1014. URL <https://arc.aiaa.org/doi/10.2514/6.2018-1014>
- [43] S. Y. Yusuf, D. Hayes, A. Pontillo, M. A. Carrizales, G. X. Dussart, M. M. Lone, *Aeroelastic Scaling for Flexible High Aspect Ratio Wings*, in: AIAA Scitech 2019 Forum, American Institute of Aeronautics and Astronautics, Reston, Virginia, 2019, pp. 1–14. doi:10.2514/6.2019-1594. URL <https://arc.aiaa.org/doi/10.2514/6.2019-1594>
- [44] D. Hayes, A. Pontillo, S. Y. Yusuf, M. M. Lone, J. Whidborne, *High aspect ratio wing design using the minimum exergy destruction principle*, in: AIAA Scitech 2019 Forum, American Institute of Aeronautics and Astronautics, Kissimmee, FL, 2019, p. 21. doi:10.2514/6.2019-1592. URL <https://arc.aiaa.org/doi/10.2514/6.2019-1592>
- [45] A. Pontillo, *High Aspect Ratio Wings on Commercial Aircraft: a Numerical and Experimental approach*, PhD thesis, Centre for Aeronautics, Cranfield University (2020). URL <https://dspace.lib.cranfield.ac.uk/handle/1826/20266>
- [46] G. Dessena, *Identification of flexible structures dynamics*, PhD thesis, Centre for Autonomous and Cyber-Physical Systems, Cranfield University (2023). URL <https://dspace.lib.cranfield.ac.uk/handle/1826/20261>
- [47] S. Y. Yusuf, *On Scaling and System Identification and Dynamic Scaling of a Flexible Aircraft*, Phd thesis, Centre for Aeronautics, Cranfield University (2019). URL <https://dspace.lib.cranfield.ac.uk/handle/1826/20037>
- [48] G. Dessena, M. Civera, A. Pontillo, D. I. Ignatyev, J. F. Whidborne, L. Zanotti Fragonara, *Noise-robust modal parameter identification and damage assessment for aero-structures*, Aircraft Engineering and Aerospace Technology 96 (11) (2024) 27–36. doi:10.1108/AEAT-06-2024-0178. URL <https://www.emerald.com/insight/content/doi/10.1108/AEAT-06-2024-0178/full/html>
- [49] N. P. Macdonald, J. M. Cabot, P. Smejkal, R. M. Guijt, B. Paull, M. C. Breadmore, *Comparing microfluidic performance of three-dimensional (3D) printing platforms*, Analytical Chemistry 89 (7) (2017) 3858–3866. doi:10.1021/acs.analchem.7b00136. URL <https://pubs.acs.org/doi/10.1021/acs.analchem.7b00136>
- [50] A. J. Keane, A. Sóbester, J. P. Scanlan, *Small Unmanned Fixed-wing Aircraft Design*, Wiley, Chichester, UK, 2017. doi:10.1002/9781119406303. URL <https://onlinelibrary.wiley.com/doi/book/10.1002/9781119406303>
- [51] D. M. J. Dykstra, S. Janbaz, C. Coulais, *The extreme mechanics of viscoelastic metamaterials*, APL Materials 10 (8) (aug 2022). doi:10.1063/5.0094224. URL <https://pubs.aip.org/apm/article/10/8/080702/2834983/The-extreme-mechanics-of-viscoelastic>
- [52] A. Bossart, D. M. J. Dykstra, J. van der Laan, C. Coulais, *Oligomodal metamaterials with multifunctional mechanics*, Proceedings of the National Academy of Sciences 118 (21) (may 2021). doi:10.1073/pnas.2018610118. URL <https://pnas.org/doi/full/10.1073/pnas.2018610118>
- [53] G. Dessena, D. I. Ignatyev, J. F. J. Whidborne, A. Pontillo, L. Zanotti Fragonara, L. Fragonara, *Ground vibration testing of a high aspect ratio wing with revolving clamp*, in: 33rd Congress of the International Council of the Aeronautical Sciences, ICAS 2022, Vol. 6, International Council of the Aeronautical Sciences, Stockholm, Sweden, 2022, pp. 4169–4181. doi:10.17862/cranfield.rd.20486229. URL [https://www.icas.org/ICAS\\_ARCHIVE/ICAS2022/data/papers/ICAS2022\\_0644\\_paper.pdf](https://www.icas.org/ICAS_ARCHIVE/ICAS2022/data/papers/ICAS2022_0644_paper.pdf)
- [54] F. Dezi, F. Gara, D. Roia, *Dynamic Characterization of Open-ended Pipe Piles in Marine Environment*, in: Applied Studies of Coastal and Marine Environments, InTech, 2016, Ch. 8, pp. 169–204. doi:10.5772/62055. URL <https://www.intechopen.com/chapters/49784>
- [55] F. R. Spitznogle, A. H. Quazi, *Representation and Analysis of Time-Limited Signals Using a Complex Exponential Algorithm*, The Journal of the Acoustical Society of America 47 (5A) (1970) 1150–1155. doi:10.1121/1.1912020. URL <https://pubs.aip.org/jasa/article/47/5A/1150/716351/Representation-and-Analysis-of-Time-Limited>
- [56] F. R. Spitznogle, J. M. Barrett, C. I. Black, T. W. Ellis, W. L. LaFuze, *Representation and analysis of sonar signals. Volume I. Improvements in the Complex Exponential signal analysis computational algorithm.*, Tech. rep., Office of Naval Research- Contract No. N00014-69-C0315, 1971 (1971). URL <https://apps.dtic.mil/sti/citations/AD0885563>